Stigmatic spectrometers for extended sources: design with toroidal varied-line-space gratings

Luca Poletto and Roger J. Thomas

Performances are presented of three classes of imaging slit spectrometers for extended sources with aberration-corrected gratings. A general analytical expression for minimizing off-axis grating aberrations is obtained, and it is demonstrated that these aberrations are minimized when the spectrometer is operated at a magnification higher than unity. Classical designs with toroidal uniform-line-spaced (TULS) or spherical varied-line-space (SVLS) gratings are compared with a new class of designs that utilize toroidal varied-line-space (TVLS) gratings. Although TULS and SVLS designs with two stigmatic points can be designed to operate at near-unity magnification with excellent on-axis spectral and spatial resolutions, they cannot be made to satisfy the general off-axis condition, and so their off-axis performances are not optimum. On the contrary TVLS designs with two stigmatic points can be operated at almost any magnification, thus satisfying the off-axis condition perfectly. Such designs are suitable for imaging spectrometer observations that require an extended field of view.

OCIS codes: 050.1950, 080.1010, 220.1000, 120.6200.

1. Introduction

A typical slit spectrometer has an intrinsic spatial-resolution capability only in the plane perpendicular to the spectral dispersion plane; i.e., a single acquisition gives the spatial distribution of an extended source only in the direction parallel to the entrance slit. In a so-called stigmatic spectrometer the optical aberrations are corrected both on the spectral dispersion plane, perpendicular to the entrance slit, and on the cross plane, parallel to the entrance slit.[1] In this way a pointlike source on the entrance slit is reimaged as a spectrally dispersed point on the focal plane. Two-dimensional monochromatic images can then be obtained by moving the spectrometer in the direction perpendicular to the entrance slit and taking a set of consecutive acquisitions.

The aberrations of an optical system are at a minimum for sources placed on the optical axis of the instrument, usually the center of the entrance slit, and in general they grow larger with the increasing distance from the optical axis, i.e., for the so-called off-plane sources. In the case of an imaging spectrometer, this means that both the degree of monochromaticity and the spatial resolution of an image decrease far from the optical axis. The scientific requirements on the spectral and the spatial resolutions are then satisfied only over a limited field of view.

When one is designing a normal-incidence stigmatic spectroscopic instrument, aberration-corrected concave gratings are often used.[2] The simplest such spectrometer consists of a single optical element, namely, the grating, which provides both spectral dispersion and spatial reimaging of the entrance slit. Single-reflection designs also give the highest spectrometer efficiency, an extremely important consideration in the extreme ultraviolet (EUV) spectral region, where normal-incidence reflectivity is rather low.

Two main approaches have been used in the past for correcting the optical aberrations in single-reflection spectrometers: uniform-line-spaced (ULS) gratings ruled on an aspherical blank[3] or varied-line-space (VLS) gratings ruled on a spherical blank.[4]

In the former case the groove spacing is constant and the aberrations are corrected by the aspherical surface of the grating: A toroidal blank is usually adopted for realizing the coincidence of the spectral and spatial focal curves over the bandpass of interest

L. Poletto is with Laboratory for UV and X-Ray Optical Research, Department of Information Engineering, Instituto Nazionale per la Fisica della Materia, University of Padova, via Gradenigo 6/B-35131, Padova, Italy (e-mail, poletto@dei.unipd.it). R. J. Thomas is with Laboratory for Astronomy and Solar Physics, Code 682, NASA Goddard Space Flight Center, Greenbelt, Maryland 20771.

Received 8 October 2003; accepted 10 December 2003.
0003-6935/04/102029-10$15.00/0

by using a different radius of curvature in the sagittal direction rather than in the tangential one. In this way the spatial focal curve can be made to intersect the spectral focal curve, that is, the Rowland circle, at one or two points.

On a VLS grating the groove spacing changes along the surface following a polynomial law: In such a system aberrations can be controlled by adjusting the parameters for ruling variations. When the proper distribution of line spacing is chosen, the spectral focal curve can be brought to intersect the spatial focal curve at one or two points.[5] Moreover it can be shown that a VLS grating ruled on a spherical varied-line-space (SVLS) surface is superior to the equivalent ULS grating ruled on a toroidal uniform-line-space (TULS) surface in terms of off-axis performance.[6]

Both the classical TULS design and the more recent SVLS design have been successfully adopted for observations of EUV extended sources, both in laboratory and in space applications.[7–10]

A logical extension of the concepts described above has been the recent suggestion to rule VLS grooves on an aspherical (toroidal) surface, producing a toroidal varied-line-space (TVLS) grating.[11] An additional design parameter, namely, the sagittal radius, is then available to control imaging aberrations and to optimize the off-axis performance. Such TVLS gratings have been found to provide excellent off-axis imaging in configurations with magnification higher than unity, permitting high-quality performance in compact instrument packages. TVLS designs have recently been proposed for a number of UV and EUV spectrometers looking at the solar disk.

In this paper the off-axis performances of imaging slit spectrometers with aberration-corrected gratings are presented. The general analytical expression for minimizing the off-axis grating aberrations, then maximizing the useful field of view of the spectrometer, is obtained in Section 2: It is demonstrated that off-axis aberrations are minimized when the spectrometer is operated at a magnification different from unity. Classical TULS and SVLS designs, with two stigmatic points within the observed spectral region, do not fulfill this condition, being operated at a magnification near unity: They have excellent on-axis spectral and spatial resolutions but degrading off-axis performances. In general the off-axis condition can be perfectly met by TULS or SVLS designs only if there is just one stigmatic point within the spectral region to be observed; in this case the useful field of view is increased, but the bandpass over which the instrument can operate is severely reduced. On the contrary the additional free parameter of the TVLS design, namely, the sagittal grating radius, allows spectrometers with two stigmatic points within its spectral bandpass and with a magnification higher than unity that fulfills the off-axis condition, giving a large stigmatic FOV throughout an extended spectral region. Finally, the design of a spectrometer for high-resolution observations of the solar corona over a wide spectral region and extended field of view is presented in Section 3: It is shown that the TVLS design gives a distinctly better performance in terms of its off-axis imaging capabilities.

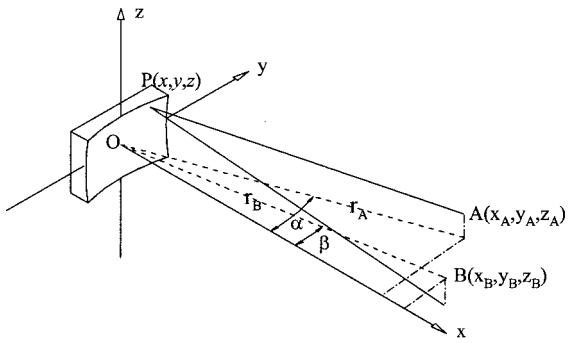

Fig. 1. Schematic of the optical layout of a concave grating.

2. Concave Gratings for Stigmatic Imaging

A. Condition for Minimum Off-Axis Aberrations

The design principle of a spectrometer with an aberration-corrected grating has been well established.[12] The optical layout of a concave grating is shown in Fig. 1 with a rectangular coordinate system: The origin, O, is on the grating vertex; the x axis is normal to the surface at the origin point; and the y and z axes are, respectively, perpendicular and parallel to the grooves. The source is placed at point A (x_A, y_A, z_A) on the entrance-slit plane, and point B (x_B, y_B, z_B) is the nominal focal point of wavelength λ diffracted in the mth order by the grating. The generic point, P (x, y, z), spans over the whole grating surface.

The groove density along the grating surface is expressed as

$$\sigma(y) = \sigma_0 + \sigma_1 y + \sigma_2 y^2 + \sigma_3 y^3, \tag{1}$$

where σ_0 is the central groove density (i.e., for $y = 0$) and σ_1, σ_2, σ_3 are the parameters for ruling variations. In the case of a ULS grating, $\sigma_1 = \sigma_2 = \sigma_3 = 0$; so the groove density is constant along the surface, $\sigma(y) = \sigma_0$.

The relationship between the geometrical parameters of the optical layout (entrance arm r_A, exit arm r_B, incidence angle α, and diffraction angle β), the grating parameters (tangential radius R and sagittal radius ρ, where $\rho = R$ for spherical gratings), and the coefficients for groove-space variation (σ_1, σ_2, and σ_3) is found by expressing the light-path function F as a power series of y and z:

$$\begin{aligned} F &= r_A + r_B + \sum_{i,j} y^i z^j F_{ij} \\ &= r_A + r_B + \sum_{i,j} y^i z^j (C_{ij} + m\lambda\sigma_0 M_{ij}), \end{aligned} \tag{2}$$

where either index i or j must be greater than zero, so that the first terms of the series are F_{10} and F_{01}.

The C_{ij} terms depend only on the geometry of the grating. The complete terms of the series up to sec-

ond order and the main third- and fourth-order terms are[3]

$$C_{10} = -\sin\alpha\left(1 - \frac{z_A^2}{2r_A^2}\right) - \sin\beta\left(1 - \frac{z_B^2}{2r_B^2}\right), \tag{3}$$

$$C_{01} = -\frac{z_A}{r_A} - \frac{z_B}{r_B}, \tag{4}$$

$$C_{20} = \frac{1}{2}\left(\frac{\cos^2\alpha}{r_A} + \frac{\cos^2\beta}{r_B} - \frac{\cos\alpha + \cos\beta}{\mathrm{R}}\right) + \frac{z_A^2}{2r_A^2}\left(\frac{\sin^2\alpha}{r_A} - \frac{\cos^2\alpha}{r_A} + \frac{\cos\alpha}{2\mathrm{R}}\right) + \frac{z_B^2}{2r_B^2}\left(\frac{\sin^2\beta}{r_B} - \frac{\cos^2\beta}{r_B} + \frac{\cos\beta}{2\mathrm{R}}\right), \tag{5}$$

$$C_{02} = \frac{1}{2}\left(\frac{1}{r_A} + \frac{1}{r_B} - \frac{\cos\alpha + \cos\beta}{\rho}\right) - \frac{z_A^2}{4r_A^2}\left(\frac{3}{r_A} - \frac{\cos\alpha}{\rho}\right) - \frac{z_B^2}{4r_B^2}\left(\frac{3}{r_B} - \frac{\cos\beta}{\rho}\right), \tag{6}$$

$$C_{11} = -\sin\alpha\,\frac{z_A}{r_A^2} - \sin\beta\,\frac{z_B}{r_B^2}, \tag{7}$$

$$C_{30} = \frac{1}{2}\frac{\sin\alpha}{r_A}\left(\frac{\cos^2\alpha}{r_A} - \frac{\cos\alpha}{R}\right) + \frac{1}{2}\frac{\sin\beta}{r_B}\left(\frac{\cos^2\beta}{r_B} - \frac{\cos\beta}{R}\right), \tag{8}$$

$$C_{40} = \frac{\sin^2\alpha}{2r_A^2}\left(\frac{\cos^2\alpha}{r_A} - \frac{\cos\alpha}{R}\right) + \frac{1}{8R^2}\left(\frac{1}{r_A} - \frac{\cos\alpha}{R}\right) - \frac{1}{8r_A^2}\left(\frac{\cos^2\alpha}{r_A} - \frac{\cos\alpha}{R}\right)^2 + \frac{\sin^2\beta}{2r_B^2}\left(\frac{\cos^2\beta}{r_B} - \frac{\cos\beta}{R}\right) + \frac{1}{8R^2}\left(\frac{1}{r_B} - \frac{\cos\beta}{R}\right) - \frac{1}{8r_B^2}\left(\frac{\cos^2\beta}{r_B} - \frac{\cos\beta}{R}\right)^2. \tag{9}$$

The coefficients M_{ij} depend on the groove-space variations. In the case of ULS gratings, all but M_{10} are zero:

$$M_{10} = 1, \qquad M_{ij} = 0 \text{ for } i, j \neq 1, 0, \tag{10}$$

whereas in the case of VLS gratings the nonzero terms are[4]

$$M_{10} = 1, \qquad M_{20} = \sigma_1/2\sigma_0, \qquad M_{30} = \sigma_2/3\sigma_0, \qquad M_{40} = \sigma_3/4\sigma_0. \tag{11}$$

According to Fermat's principle of least time, the image point, B, is located such that the light-path function will be an extreme for any point P spanning over the grating surface. Stigmatic spectral image focusing is then obtained setting the derivative with respect to the variables y and z equal to zero, i.e., $\partial F/\partial y = \partial F/\partial z = 0$. The latter condition must be satisfied simultaneously by any pair of y and z on the surface of the grating for fixed point B: This is realized by setting all coefficients of the power series in Eq. (2) equal to zero.

When F_{01} is set equal to zero, the fundamental equation

$$\frac{z_A}{r_A} = -\frac{z_B}{r_B} \tag{12}$$

is obtained, which gives the grating image magnification.

When F_{10} is set equal to zero and Eq. (12) is used, the grating equation

$$(\sin\alpha + \sin\beta)\left(1 - \frac{z_A^2}{2r_A^2}\right) = m\lambda\sigma_0 \tag{13}$$

is obtained, giving the relationship between the wavelength of the incoming radiation, the central groove density, and the direction of the incident and the diffracted rays. The signs of α and β are opposite if A and B lie on different sides of the x–z plane.

The F_{20}, F_{02}, and F_{11} terms control defocusing, the main optical aberration limiting the spectral and spatial resolution. The F_{20} term shows the spectral defocusing in the spectral dispersion plane, which increases linearly with the width of the grating illuminated area (i.e., the grating size perpendicular to the grooves). The F_{02} term shows the spatial defocusing in the plane perpendicular to the spectral dispersion, which increases linearly with the height of the grating illuminated area (i.e., the grating size parallel to the grooves). The F_{11} term is null for on-axis sources and gives off-axis defocusing in both the spectral and the spatial directions. The terms are given by

$$F_{20} = \frac{1}{2}\left(\frac{\cos^2\alpha}{r_A} + \frac{\cos^2\beta}{r_B} - \frac{\cos\alpha + \cos\beta}{\mathrm{R}} + m\lambda\sigma_1\right) + \frac{z_A^2}{2r_A^2}\left(\frac{\sin^2\alpha}{r_A} - \frac{\cos^2\alpha}{r_A} + \frac{\sin^2\beta}{r_B} - \frac{\cos^2\beta}{r_B} + \frac{\cos\alpha + \cos\beta}{2R}\right), \tag{14}$$

$$F_{02} = \frac{1}{2}\left(\frac{1}{r_A} + \frac{1}{r_B} - \frac{\cos\alpha + \cos\beta}{\rho}\right) - \frac{z_A^2}{4r_A^2}\left(\frac{3}{r_A} - \frac{3}{r_B} - \frac{\cos\alpha + \cos\beta}{\rho}\right), \tag{15}$$

$$F_{11} = -\frac{z_A}{r_A}\left(\frac{\sin\alpha}{r_A} - \frac{\sin\beta}{r_B}\right). \tag{16}$$

Usually a design is optimized for the best on-axis performance. In this case z_A is set equal to zero, and equations $F_{20} = 0$ and $F_{02} = 0$ give, respectively, the spectral and spatial focal curves, defining the surfaces on which spectral or spatial defocusing are zero. The aim of the optical design of a stigmatic spectrom-

eter is to realize the coincidence of the spectral and spatial focal curves over the wavelength region of interest. It is impossible to realize a perfect overlap of the two curves over the whole spectral region to be acquired, but the spectral focal curve can be brought to intersect the spatial focal curve at one or two points, which then define the so-called stigmatic wavelengths. Around each of these points the spectrometer is almost stigmatic over a region whose extension depends primarily on beam divergence.

Once the stigmatic design has been chosen, the on-axis defocusing is minimized, but the F_{20}, F_{02}, and F_{11} terms are different from zero for off-axis sources ($z_A \neq 0$). The off-axis defocusing is dominated by the F_{11} term, which is proportional to $1/r^2$, while the F_{20} and F_{02} terms are proportional to $1/r^3$. By setting F_{11} equal to zero, the condition for minimizing the off-axis grating aberrations is obtained:

$$\frac{\sin \beta}{\sin \alpha} = \frac{r_B}{r_A} = M, \tag{17}$$

where M is the spectrometer magnification r_B/r_A. [There is no relationship between magnification M and the light-path coefficients M_{ij} reported in Eqs. (10) and (11).] A grating spectrometer has a minimum of off-axis aberrations where the ratio between the diffraction and the incidence angles is equal to the instrument magnification. Note that this condition is independent of the grating type (if ULS or VLS) and of the grating geometry (if spherical or aspherical): It is a general condition for maximizing the off-axis grating performance of any imaging spectrometer.

It is clear from Eq. (17) that a spectrometer working with unity magnification gives the best off-axis performance when $\beta = \alpha$. But this is not a feasible condition because of the interference between the entrance slit and detector. Designs with unity magnification with β as close as possible to α (i.e., a small subtended angle α–β) are expected to give better off-axis performances than designs with a larger grating subtended angle. However, given that actual slits and detectors must have some physical size, Eq. (17) can be exactly fulfilled only by spectrometers operating at a magnification different from unity.

Both TULS and SVLS designs can be adopted with a magnification higher than unity in configurations with only a single stigmatic wavelength by choosing an incidence angle α according to Eq. (17) combined with Eq. (13). If the spectral region to be acquired is sufficiently narrow and/or the beam divergence is low, the on-axis performance can be good enough to satisfy the scientific requirements while also providing excellent off-axis performance. TULS and SVLS designs can also be adopted that operate at magnification higher than unity with two stigmatic wavelengths, but once the incidence angle α is chosen according to Eq. (17) to minimize the off-axis aberrations, the remaining parameters are not enough for one to choose the location of the stigmatic points anywhere within the observed spectral region.

In the following designs with two stigmatic wavelengths within the operating bandpass are presented with particular attention to their off-axis performances.

B. Design of the Toroidal Uniform-Line-Spaced Grating

The conventional approach to designing a normal-incidence stigmatic spectrometer has been to use TULS gratings.[3] We express the conditions for spectral and spatial on-axis focusing, respectively, by

$$\frac{\cos^2 \alpha}{r_A} + \frac{\cos^2 \beta}{r_{Bh}} - \frac{\cos \alpha + \cos \beta}{R} = 0 \quad \text{spectral focal curve,} \tag{18}$$

$$\frac{1}{r_A} + \frac{1}{r_{Bv}} - \frac{\cos \alpha + \cos \beta}{\rho} = 0 \quad \text{spatial focal curve,} \tag{19}$$

which are derived from Eqs. (14) and (15), noting that $\sigma_1 = z_A = 0$ in this case. Here r_{Bh} and r_{Bv} indicate the lengths of the exit arm that produce the best spectral and spatial on-axis focusing, respectively. Equation (18) is satisfied for each angle α and β by

$$r_A = R \cos \alpha, \qquad r_{Bh} = R \cos \beta, \tag{20}$$

which is the equation of the Rowland circle, i.e., the circle tangent to the grating in the origin point, O, and having a diameter equal to the grating tangential radius R. The spatial focal curve can intersect the spectral focal curve for two stigmatic wavelengths λ_1 and λ_2 within the desired bandpass, diffracted, respectively, at angles β_1 and β_2, if the sagittal radius ρ is chosen accordingly to

$$\rho = R \cos \alpha \cos \beta_1 = R \cos \alpha \cos \beta_2, \tag{21}$$

where

$$\beta_1 = -\beta_2 = \text{a sin}\left(m\sigma_0 \frac{\lambda_1 - \lambda_2}{2}\right), \tag{22}$$

$$\alpha = a \sin\left(m\sigma_0 \frac{\lambda_1 + \lambda_2}{2}\right) = \text{a sin}(m\sigma_0\lambda_c), \tag{23}$$

so that the central wavelength $\lambda_c = (\lambda_1 + \lambda_2)/2$ is diffracted at $\beta_c = 0$.

The magnification of the conventional TULS design is slightly higher than unity and almost constant within the spectral region to be acquired, $M \approx 1/\cos \alpha > \approx 1$; so the condition for the best off-axis performance is $\alpha \approx \beta$, which cannot be achieved. Therefore such TULS designs cannot be fully optimized for the observations of extended sources. Lower off-axis aberrations are expected for the highest wavelengths in the spectral region to be observed, where the subtended angle α–β is smaller.

TULS designs are possible with two stigmatic wavelengths even at magnifications higher than unity, but they have limitations. Let M_c indicate the magnification at the central wavelength of the spec-

tral interval to be acquired, defined as $M_c = r_{Bh}(\beta_c)/r_A$. The incidence angle has to be chosen according to Eq. (23). The tangential grating radius is chosen from Eq. (18) as

$$R = r_A M_c \frac{\cos\alpha + \cos\beta_c}{M_c \cos^2\alpha + \cos^2\beta_c}, \tag{24}$$

and the sagittal radius has to be chosen as

$$\rho = \cos^2\beta_1\left(\frac{1}{R} - \frac{\cos\alpha + \cos\beta_1}{r_A}\right)^{-1} = \cos^2\beta_2\left(\frac{1}{R} - \frac{\cos\alpha + \cos\beta_2}{r_A}\right)^{-1}. \tag{25}$$

Again Eq. (17) is not met; so the off-axis performance is not optimized. To satisfy Eq. (17) at a certain wavelength, the incidence angle has to be chosen closer to zero than the value found by Eq. (23), and then the corresponding diffraction angle moves apart from zero. Since the two stigmatic wavelengths are those diffracted at symmetric angles (i.e., $\beta_1 = -\beta_2$), it is clear that only the stigmatic wavelength diffracted at the positive angle falls into the spectral interval to be acquired. In general, when the incidence angle is moved toward zero to get closer to Eq. (17), the two stigmatic wavelengths move farther apart until one of them is shifted entirely out of the spectral region of interest.

C. Design of the Spherical Varied-Line-Space Grating

When a SVLS grating is used, the spectral and spatial focal curves are determined by

$$\frac{\cos^2\alpha}{r_A} + \frac{\cos^2\beta}{r_{Bh}} - \frac{\cos\alpha + \cos\beta}{R} + m\lambda\sigma_1 = 0 \quad \text{spectral focal curve,} \tag{26}$$

$$\frac{1}{r_A} + \frac{1}{r_{Bv}} - \frac{\cos\alpha + \cos\beta}{R} = 0 \quad \text{spatial focal curve.} \tag{27}$$

Equation (27) is satisfied by

$$r_A = \frac{R}{\cos\alpha}, \qquad r_{Bv} = \frac{R}{\cos\beta}, \tag{28}$$

which gives the equation of a line tangent to the Rowland circle where spatial defocusing is zero.

In the design of a SVLS grating spectrometer the usually adopted optical layout, initially proposed by Harada, has the entrance slit at the position given by Eq. (28). The detector surface is put on the spatial focal curve; the angle of incidence α and the ruling parameter σ_1 are then determined, making the spectral focal curve intersect the spatial focal curve at the two stigmatic wavelengths, λ_1 and λ_2.[6] This is achieved by selecting angle α by the relation

$$(\sin\beta_1 - \sin\beta_2)\cos\alpha\sin^2\alpha + (\sin\alpha + \sin\beta_1)\cos\beta_2\sin^2\beta_2 - (\sin\alpha + \sin\beta_2)\cos\beta_1\sin^2\beta_1 = 0. \tag{29}$$

The ruling parameter σ_1 is then determined by Eq. (26). Furthermore it can be shown that the additional parameters for ruling variations, σ_2 and σ_3, can be determined to minimize on-axis astigmatic coma and spherical aberration.[6]

The magnification of the SVLS design is slightly lower than unity, $M = \cos\alpha/\cos\beta <\approx 1$, so again the condition for the best off-axis performance is $\alpha \approx \beta$ as in the TULS case, which again is not possible. However, it can be shown that the optimum incidence angle α determined by Eq. (29) for the SVLS design is lower than the corresponding TULS design; so the subtended angle α–β is closer to zero. This means that the off-axis performance of the SVLS system will then be superior to the equivalent TULS system. On the other hand, SVLS configurations may have problems of accommodation, since the minimum subtended angle can be so small as to cause interference between the entrance slit and the detector. Then the incidence angle has to be increased, so that Eq. (29) is no longer satisfied. In such cases, some performance degradations both on axis and off axis have to be accepted.

The SVLS design can also be used in configurations with magnifications higher than unity with two stigmatic wavelengths. The incidence angle α has to be selected by

$$\frac{\cos\alpha + \cos\beta_1}{\sin\alpha + \sin\beta_1}\left(\frac{1 + M_c}{M_c}\frac{\sin^2\beta_1}{\cos\alpha + \cos\beta_c} - \cos\alpha + \cos\beta_1\right) - \frac{\cos\alpha + \cos\beta_2}{\sin\alpha + \sin\beta_2}\left(\frac{1 + M_c}{M_c}\frac{\sin^2\beta_2}{\cos\alpha + \cos\beta_c} - \cos\alpha + \cos\beta_2\right) = 0, \tag{30}$$

where the spherical grating radius is given from Eq. (27) by

$$R = r_A(\cos\alpha + \cos\beta_c)\frac{M_c}{1 + M_c}, \tag{31}$$

and the ruling parameter σ_1 is determined by Eq. (26).

It can be shown that the incidence angle as calculated by Eq. (30) is closer to the angle satisfying Eq. (17) than the corresponding incidence angle for the TULS design. Again, the off-axis performance of the SVLS system is superior to the equivalent TULS system.

Equation (17) can be satisfied at one wavelength

within the design bandpass if the incidence angle chosen is closer to zero than the value found by Eq. (30). As in the TULS case, when the incidence angle is moved toward zero, the two stigmatic wavelengths move farther apart, until one of them is shifted entirely out of the observed spectral range.

D. Design of the Toroidal Varied-Line-Space Grating

Both TULS and SVLS designs can be adopted in configurations with magnification higher than unity and minimum off-axis aberrations, as stated by Eq. (17), but then only for a single stigmatic wavelength within the bandpass. If two stigmatic wavelengths and the exact fulfillment of Eq. (17) are simultaneously required, an additional parameter has to be introduced into the optical design. This can be done with TVLS gratings, where the new parameter is the grating sagittal radius ρ.

The initial parameters to be fixed are the two stigmatic wavelengths, λ_1 and λ_2; the entrance arm r_A; the magnification M_c at the central wavelength, $\lambda_c = (\lambda_1 + \lambda_2)/2$; and the grating central groove density σ_0. The incidence angle α is calculated to verify Eq. (17) at wavelength λ_c:

$$\alpha = a \sin\left(\frac{m\lambda_c\sigma_0}{1 + M_c}\right). \tag{32}$$

The spectral and spatial focal curves are determined by

$$\frac{\cos^2 \alpha}{r_A} + \frac{\cos^2 \beta}{r_{Bh}} - \frac{\cos \alpha + \cos \beta}{R} + m\lambda\sigma_1 = 0$$

spectral focal curve, (33)

$$\frac{1}{r_A} + \frac{1}{r_{Bv}} - \frac{\cos \alpha + \cos \beta}{\rho} = 0$$

spatial focal curve. (34)

The grating sagittal radius is calculated by

$$\rho = r_A(\cos \alpha + \cos \beta_c)\frac{M_c}{1 + M_c}. \tag{35}$$

The next two parameters, R and σ_1, are calculated to have the spectral focal curve intersecting the spatial focal curve at the two stigmatic wavelengths, λ_1 and λ_2:

$$R = \frac{\lambda_1(\cos \alpha + \cos \beta_2) - \lambda_2(\cos \alpha + \cos \beta_1)}{\lambda_1 K_2 - \lambda_2 K_1}, \tag{36}$$

$$\sigma_1 = \frac{1}{m}\frac{K_2(\cos \alpha + \cos \beta_1) - K_1(\cos \alpha + \cos \beta_2)}{\lambda_1(\cos \alpha + \cos \beta_2) - \lambda_2(\cos \alpha + \cos \beta_1)}, \tag{37}$$

where

$$K_1 = \frac{\cos^2 \alpha}{r_A} + \cos^2 \beta_1\left(\frac{\cos \alpha + \cos \beta_1}{\rho} - \frac{1}{r_A}\right), \tag{38}$$

$$K_2 = \frac{\cos^2 \alpha}{r_A} + \cos^2 \beta_2\left(\frac{\cos \alpha + \cos \beta_2}{\rho} - \frac{1}{r_A}\right). \tag{39}$$

We can determine the additional parameters for ruling variations, σ_2 and σ_3, to minimize on-axis astigmatic coma and spherical aberration at the central wavelength λ_c:

$$\sigma_2 = -\frac{3}{2m\lambda_C}\left[\frac{\sin \alpha \cos \alpha}{r_A}\left(\frac{\cos \alpha}{r_A} - \frac{1}{R}\right) + \frac{\sin \beta_C \cos \beta_C}{r_{Bh}}\left(\frac{\cos \beta_C}{r_{Bh}} - \frac{1}{R}\right)\right], \tag{40}$$

$$\sigma_3 = -\frac{1}{2m\lambda_C}\left[\frac{4 \sin^2 \alpha \cos \alpha}{r_A^2}\left(\frac{\cos \alpha}{r_A} - \frac{1}{R}\right) - \frac{\cos^2 \alpha}{r_A}\left(\frac{\cos \alpha}{r_A} - \frac{1}{R}\right)^2 + \frac{1}{R^2}\left(\frac{1}{r_A} - \frac{\cos \alpha}{R}\right) + \frac{4 \sin^2 \beta_C \cos \beta_C}{r_{Bh}^2}\left(\frac{\cos \beta_C}{r_{Bh}} - \frac{1}{R}\right) - \frac{\cos^2 \beta_C}{r_{Bh}}\left(\frac{\cos \beta_C}{r_{Bh}} - \frac{1}{R}\right)^2 + \frac{1}{R^2}\left(\frac{1}{r_{Bh}} - \frac{\cos \beta_C}{R}\right)\right]. \tag{41}$$

Finally the detector surface has to be on the plane that best fits the spectral and the spatial focal curves given above.

Equations (32), (35), (36), (37), (40), and (41) define completely the TVLS design with a magnification higher than unity, two stigmatic points, and minimum off-axis aberrations.

3. Ray-Tracing Simulations

It has just been shown that TVLS designs can be adopted for high-resolution observations of extended sources in configurations with magnification different from unity. As one of the main fields of application, this new design concept can be applied to space instrumentation for EUV spectroscopic observations of the solar corona. If simultaneous high-resolution observations of EUV emissions from different regions of the corona are required, the spectral region to be acquired becomes wide and the length of the spectrum on the focal plane may require more than one detector. An extended spatial field of view (i.e., in the direction parallel to the spectrometer entrance slit) is also necessary for one to look simultaneously at an area on the Sun that is as wide as possible.

A typical instrument normally consists of a telescope feeding a grating spectrometer through an entrance slit; so the global spectral and spatial performances have to be determined by taking into account the contributions of both optical components (i.e., telescope and spectrometer) to the optical transfer function. A telescope spectrometer has three main optical parameters that determine its performance, namely, the spatial resolution in the direction perpendicular to the entrance slit, the spectral resolution, and the spatial resolution in the direction parallel to the entrance slit. The first depends only on the telescope design, the second only on the spectrom-

Table 1. General Characteristics of the EUV Spectrometer

Parameters	Values
Wavelength	115–130 nm 140–155 nm
Field of view parallel to the slit	30 arc min
Spatial resolution parallel to the slit	1 arc sec
Spatial resolving element (perpendicular to the slit)	1 arc sec/pixel
Spectral resolving element	8 pm/pixel
Pixel size	15 μm
Detector format	1800 pixel × 1800 pixel
Detector area	27 mm × 27 mm
Number of detectors	2

Table 2. Characteristics of the TULS Spectrometer

Parameters	Values
Telescope	Double-element design
Focal length	3000 mm
Entrance diameter	150 mm
Slit size	15 μm × 27 mm
Spectrometer	TULS grating
Groove density	1800 lines/mm
Stigmatic wavelengths	120 and 150 nm
Tangential radius	1000 mm
Sagittal radius	969.7 mm
Incidence angle	14.1 deg
Entrance arm	970.0 mm
Grating size	50 mm × 80 mm

eter design, and the third on both telescope and spectrometer. Several optical designs have been studied and realized for telescopes with high performance in an extended field of view: The choice of the actual design is done as a trade-off among different needs, such as for high throughput, extended field of view, low mass, and small size. Unfortunately a good telescope design contributes primarily to only one of the three optical parameters defined above (namely, the spatial resolution perpendicular to the slit); the other two are dominated by the grating performance, especially for off-axis sources.

Here TULS, SVLS, and TVLS grating configurations are compared in the design of an EUV spectrometer for high-resolution observations in a wide spectral region and extended field of view. The spectral region to be recorded has been made very wide (115–155 nm) for simultaneous diagnostics of different regions of the solar corona. If coatings on the optics and detectors are chosen for observation of the second diffracted order also, the instrument diagnostic capabilities became really huge. Two detectors are placed on the spectrometer focal plane to acquire two different spectral regions. The required field of view is 30 arc min, covering almost the full Sun from Earth orbit. The main parameters for a spectrometer operating on the first-order wavelength range of 115–155 nm are listed in Table 1. The spectral resolving element is ~0.008 nm, corresponding to a velocity resolution of 20 km/s at 120 nm, and the spatial resolving element is 1 arc sec. Each detector active area is 27 mm × 27 mm, consistent with the use of either a CCD or a microchannel plate device. Since the spectral region to be acquired consists of two different intervals on the two detectors, and a high spectral resolution is required over the whole range, an optical design with two stigmatic points has to be adopted.

A. Performance of the Toroidal Uniform-Line-Spaced Grating

The parameters of a TULS design in the Rowland configuration are listed in Table 2. The grating groove density is 1800 lines/mm, and the spectrometer arms are ~1000 mm, giving a spectral dispersion of ~0.55 nm/mm. The stigmatic wavelengths have been chosen at 120 and 150 nm. Since the grating operates at near-unity magnification, the entrance slit width has been made equal to the detector pixel size, i.e., 15 μm.

The need for a spatial resolution of 1 arc sec requires a telescope focal length of 3000 mm. A double-element telescope has been assumed, which has the disadvantage of one extra reflection over a single-mirror off-axis paraboloid system but which provides a much larger corrected field of view and a reduced length. It has been proved by ray tracing that it is possible to design a double-element telescope with aberrations lower than 15 μm over the whole field of view of 30 arc min. The spatial resolution perpendicular to the slit is then limited by the slit width to 1 arc sec. The spectral resolution and spatial resolution parallel to the slit are instead dominated by the grating performance.

A schematic drawing of the optical system is shown in Fig. 2. The two detectors have been placed at the

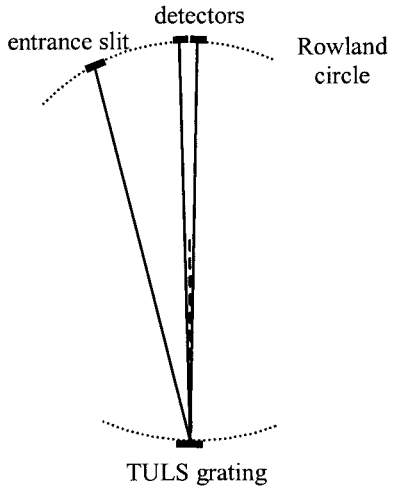

Fig. 2. Schematic of the TULS design for the 115–155-nm region. The two detectors have been placed to acquire the 115–130- and 140–155-nm spectral regions.

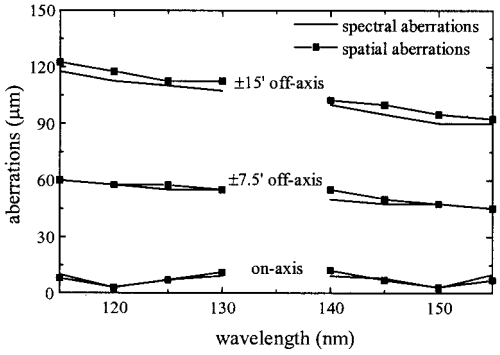

Fig. 3. FWHM aberration of the TULS design. The detector pixel size is 15 μm. The subtended angle α–β at the central wavelength is 14.1°.

best fit to the spectral and spatial focal curves and are almost normal to the direction of the incident beam. The TULS grating aberrations at FWHM are shown in Fig. 3. The spectral and spatial FWHM aberrations are lower than the pixel size for on-axis points, but they increase to as many as 8 pixels in the required extended field of view. Clearly the TULS design is not optimized for significantly extended sources.

B. Performance of the Spherical Varied-Line-Space Grating

The parameters of a comparable SVLS design in the Harada configuration are listed in Table 3. Again we assume a double-element telescope corrected over the whole field of view. The maximum groove-spacing variation is less than 1% with respect to the central groove density.

A schematic drawing of the optical system is shown in Fig. 4 with the detectors placed at the best fit to the spectral and spatial focal curves and almost normal to the direction of the incident beam. The SVLS grating FWHM aberrations are shown in Fig. 5. Since the incidence angle for the SVLS design is lower than the corresponding TULS design, the off-axis performance of the SVLS system is superior. The FWHM aberrations increase to as many as ~4 pixels in the extended field of view, corresponding to a degradation in the nominal performance by a factor of 4. When these values are compared with the 8 pixels of the off-axis aberration for the TULS design, the SVLS off-axis resolution is better by a factor of 2.

Table 3. Characteristics of the SVLS Spectrometer

Parameters	Values
Telescope	Double-element design
Focal length	3000 mm
Entrance diameter	150 mm
Slit size	15 μm × 27 mm
Spectrometer	SVLS grating
Central groove density	1800 lines/mm
Stigmatic wavelengths	120 nm and 150 nm
Radius	1000 mm
Incidence angle	9.9 degree
Entrance arm	1015.0 mm
Grating size	50 mm × 80 mm
Parameters for groove space variation	$\sigma_1 = 0.257\ \text{mm}^{-2}$
	$\sigma_2 = 5.82 \times 10^{-5}\ \text{mm}^{-3}$
	$\sigma_3 = 0$

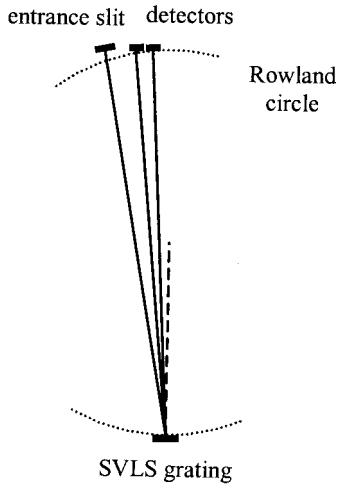

Fig. 4. Schematic of the SVLS design for the 115–155-nm region.

C. Performance of the Toroidal Varied-Line-Space Grating

Off-axis aberrations are minimized by working at a magnification higher than unity, according to Eq. (17), while maintaining both of the two stigmatic points within the spectral region to be acquired. This is made possible by designs with TVLS gratings.

When we work with unity magnification, the entrance slit width is normally kept as large as the detector pixel size. In fact, the total spectral aberrations are given by the convolution between the slit width and the residual optical aberrations on the focal plane. If the latter is lower than the pixel size and the slit width is almost equal to the pixel size, the instrumental response is limited by the detector itself and not by the optical performance.

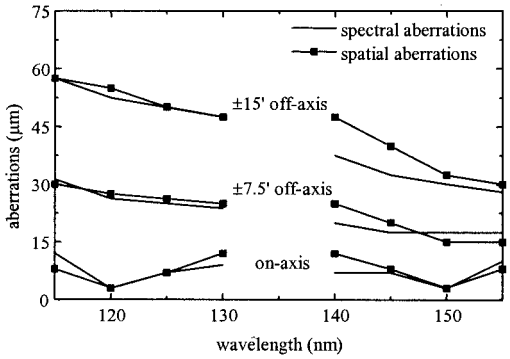

Fig. 5. FWHM aberration of the SVLS design. The detector pixel size is 15 μm. The subtended angle α–β at the central wavelength is 5.8°.

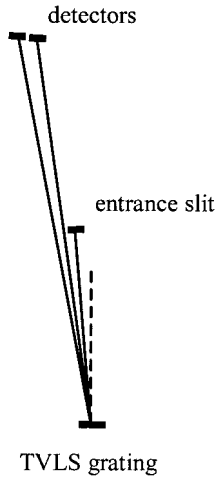

Fig. 6. Schematic drawing of the TVLS design for the 115–155-nm region.

Table 4. Characteristics of the TVLS Spectrometer

Parameters	Values
Telescope	Double-element design
Focal length	1500 mm
Entrance diameter	150 mm
Slit size	7.5 μm × 13.5 mm
Spectrometer	TVLS grating
Central groove density	1800 lines/mm
Stigmatic wavelengths	120 nm and 150 nm
Tangential radius	653.3 mm
Sagittal radius	661.2 mm
Incidence angle	4.65 degree
Entrance arm	500 mm
Medium exit arm	1000 mm
Grating size	50 mm × 65 mm
Parameters for groove space variation	$\sigma_1 = 0.565\ \text{mm}^{-2}$
	$\sigma_2 = 1.36 \times 10^{-4}\ \text{mm}^{-3}$
	$\sigma_3 = 0$

With significant magnification in the spectrometer the slit width and height must be reduced by the inverse of the magnification factor to keep them matched with the pixel size and array height of a given detector. Then the limiting consideration may become the technical question of how narrow an entrance slit can be made, although photoetching procedures for fabricating slits are now approaching sizes well below 10 μm. In the example described here the chosen magnification is 2; so the slit size has been reduced to 7.5 μm × 13.5 mm, which are feasible values.

Spectrometer magnification also means that the focal length of the telescope as well as its aberrations must be correspondingly reduced to maintain the same spatial resolution, and this gives the advantage of decreasing the length of the instrument's telescope section. The telescope design is then more challenging, but the theoretical aberrations of many double-element designs are really well below the detector pixel size. In practice the minimum slit width is often limited by the telescope's diffraction or by tolerances in the alignment. In the reported example, ray racing shows that it is possible to design a double-element telescope with a 1500-mm focal length, a 120-mm entrance aperture, and FWHM aberrations lower than 7.5 μm over the whole desired field of view. Furthermore diffraction sizes at the observed wavelengths are well below 7.5 μm.

The TVLS design parameters are listed in Table 4. The maximum groove-spacing variation is less than 1% with respect to the central groove density. A schematic drawing of the TVLS system is shown in Fig. 6. In order to best fit the spectral and spatial focal curves, the detectors have been tilted by 13 deg with respect to direction of the incident beam. The TVLS grating FWHM aberrations are shown in Fig. 7. The off-axis performance of the TVLS design is definitely better than in either the TULS or SVLS designs, the aberrations being almost lower than the pixel size over the whole field of view. For that reason the TVLS design provides constant spectral and spatial resolutions along the entire slit, another desirable feature.

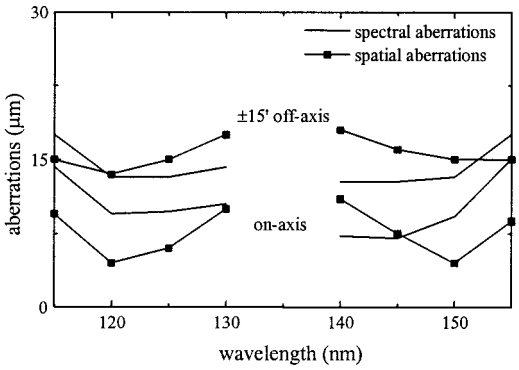

Fig. 7. FWHM aberration of the TVLS design. The detector pixel size is 15 μm. The subtended angle α–β at the central wavelength is −4.7°.

5. Conclusions

The off-axis performances of three different classes of imaging spectrometers with aberration-corrected gratings have been presented. A general analytical expression for minimizing the off-axis grating aberrations has been obtained: It has been demonstrated that such aberrations are minimized when the spectrometer is operated at a magnification higher than unity. Classical designs that use TULS or SVLS gratings with two stigmatic points have been compared with the new TVLS grating design.

The off-axis condition is not satisfied by TULS and SVLS designs that are operated at near-unity magnification. Although they show excellent on-axis spectral and spatial resolutions, their off-axis performances are therefore not optimum. On the contrary, TVLS designs with two stigmatic points are possible at almost any magnification, so they can

exactly meet the off-axis condition. These TVLS designs thus provide the best off-axis performance and so are suitable for experiments that require an extended field of view, such as solar observations, although there are potential benefits also for terrestrial and planetary remote sensing at visible and IR wavelengths.

TVLS gratings can be manufactured either by mechanical rulings or holographically. The mechanical ruling implies tight tolerances on the grating's varied spacing, which requires interferometric control of the ruling engine. Holographically, the grating can be realized by interference of properly aberrated wavefronts in the recording resist. At normal incidence the variation in the spacing is small (of the order of a few percentage points at the edges); thus the feasibility of these gratings should not be a major difficulty.

In space applications, where an instrument's size and mass are critical parameters, a TVLS design can provide excellent imaging even at very large spectrometer magnifications and beam angular apertures, giving high-quality performance and exceptional throughput in a remarkably compact physical package.

References

1. W. L. Wolfe, *Introduction to Imaging Spectrometers* (SPIE Optical Engineering Press, Bellingham, Wash., 1997).
2. J. A. R. Samson and D. L. Ederer, *Vacuum Ultraviolet Spectroscopy II* (Academic, San Diego, Calif., 1998).
3. H. Haber, "The torus grating," J. Opt. Soc. Am. **40,** 153–166 (1950).
4. T. Harada and T. Kita, "Mechanically ruled aberration-corrected concave gratings," Appl. Opt. **19,** 3987–3993 (1980).
5. T. Harada, T. Kita, S. Bowyer, and M. Hurwitz, "Design of spherical varied line-space gratings for a high-resolution EUV spectrometer," in *International Conference on the Application and Theory of Periodic Structures*, J. M. Lerner and W. R. McKinney, eds., Proc. SPIE **1545,** 2–10 (1991).
6. T. Harada, H. Sakuma, K. Takanashi, T. Watanabe, H. Hara, and T. Kita, "Design of a high-resolution extreme-ultraviolet imaging spectrometer with aberration-corrected concave gratings," Appl. Opt. **37,** 6803–6810 (1998).
7. C. Pernechele, G. Naletto, P. Nicolosi, G. Tondello, S. Fineschi, M. Romoli, G. Noci, D. Spadaro, and J. L. Kohl, "Optical performances of the UVCS/SOHO spectrometer," Appl. Opt. **36,** 813–826 (1997).
8. P. Villoresi, P. Nicolosi, and M. G. Pelizzo, "Design and experimental characterization of a high-resolution instrument for measuring the extreme-UV absorption of laser plasmas," Appl. Opt. **39,** 85–93 (2000).
9. T. Onaka, "Aberration-corrected concave grating for the Mid-Infrared Spectrometer aboard the Infrared Telescope in Space," Appl. Opt. **34,** 659–666 (1995).
10. T. Harada, H. Sakuma, T. Kita, and M. Nakamura, "Design of EUV spectrometer with stigmatic image focusing using spherical varied line-space gratings," in *X-Ray and Ultraviolet Spectroscopy and Polarimetry*, S. Fineschi, ed., Proc. SPIE **2283,** 180–188 (1994).
11. R. J. Thomas, "Toroidal varied line-space (TVLS) gratings," in *Innovative Telescopes and Instrumentation for Solar Astrophysics*, S. L. Keil and V. Avakyan, eds., Proc. SPIE **4853,** 411–418 (2002).
12. T. Namioka, "Theory of concave grating," J. Opt. Soc. Am. **49,** 446–460 (1959).